Check for updates

Magnetic structure and properties of the honeycomb antiferromagnet [Na(OH$_2$)$_3$]Mn(NCS)$_3$†

Madeleine Geers, [ab] Thomas B. Gill, [c] Andrew D. Burnett, [d] Euan N. Bassey, [‡e] Oscar Fabelo, [b] Laura Cañadillas-Delgado [b] and Matthew J. Cliffe *[a]

We report the magnetic structure and properties of a thiocyanate-based honeycomb magnet [Na(OH$_2$)$_3$]Mn(NCS)$_3$ which crystallises in the unusual low-symmetry trigonal space group $P\bar{3}$. Magnetic measurements on powder samples show this material is an antiferromagnet (ordering temperature $T_{N,mag}$ = 18.1(6) K) and can be described by nearest neighbour antiferromagnetic interactions J = −11.07(4) K. A method for growing neutron-diffraction sized single crystals (>10 mm^3) is demonstrated. Low temperature neutron single crystal diffraction shows that the compound adopts the collinear antiferromagnetic structure with $T_{N,neut}$ = 18.94(7) K, magnetic space group $P\bar{3}'$. Low temperature second-harmonic generation (SHG) measurements provide no evidence of breaking of the centre of symmetry.

Honeycomb magnets, due to their high symmetry and two-dimensionality, can host a wide range of magnetic phases, including monolayer ferromagnetism in CrI$_3$,[1] proximate Kitaev spin liquid states in RuCl$_3$ and Na$_2$Co$_2$TeO$_6$,[2,3] complex spin textures in FeCl$_3$,[4] and magnetoelectricity in Co$_2$Mo$_3$O$_8$.[5]

Molecular magnets are of particular interest for low-dimensional magnetism as it is often more straightforward to produce well-isolated low-dimensional connectivity, and the molecular ligands offer the potential for a high degree of tunability.[6] Honeycomb molecular magnets are no exception to this,

particularly those based on chelating ligands such as (ox^{2-} = C$_2$O$_4$$^{2-}$),[7–9] tetraoxolene (C$_6O_4R_2$$^{n-}$)[10] amongst others.[11,12] These structures often have multiple different paramagnetic species producing ferrimagnetic order, whether this is alternating metal sites A[M^{II}M^{III}](ox)$_3$,[7] A[M^{II}M^{III}](C$_6$O$_4$R$_2$)$_3$[13,14] or the presence of radical ligands in A$_2$[M$_2$(C$_6$O$_4$R$_2$)$_3$],[10] where A is charge balancing cation (typically alkylammonium). Equally, distorted honeycomb structures, with multiple different exchange pathways are common.[12,15,16] Examples of ideal honeycomb lattice magnets are thus comparatively rare.

One promising material family to search for honeycomb magnets are the metal thiocyanates, which show a range of low dimensional magnetic properties due to the layered structural connectivity and have interactions as strong as comparable halides.[18,19] In this paper we investigate the magnetic properties of [Na(OH$_2$)$_3$]Mn(NCS)$_3$ (NaMn(NCS)$_3$·3H$_2$O),[20] formed of ideal two-dimensional honeycomb [Mn(NCS)$_3$]$^-$ layers with the hexagonal void filled by 1D [Na(OH$_2$)$_3$]$^+$ rods [Fig. 1]. It crystallises in the low-symmetry but still trigonal $P\bar{3}$ space-group, comparatively rare in inorganic materials (fewer than 0.25% of ICSD structures[21]). As a result, the Mn(II) sites do not lie on inversion centres, which raises the possibility that magnetic

^{a} *School of Chemistry, University Park, Nottingham, NG7 2RD, UK.*
  E-mail: matthew.cliffe@nottingham.ac.uk

^{b} *Institut Laue Langevin, 71 avenue des Martyrs CS 20156, 38042 Grenoble Cedex 9, France*

^{c} *School of Electronic and Electrical Engineering, University of Leeds, LS2 9JT, UK*

^{d} *School of Chemistry, University of Leeds, Leeds, LS2 9JT, UK*

^{e} *Yusuf Hamied Department of Chemistry, University of Cambridge, Lensfield Road, Cambridge CB2 1EW, UK*
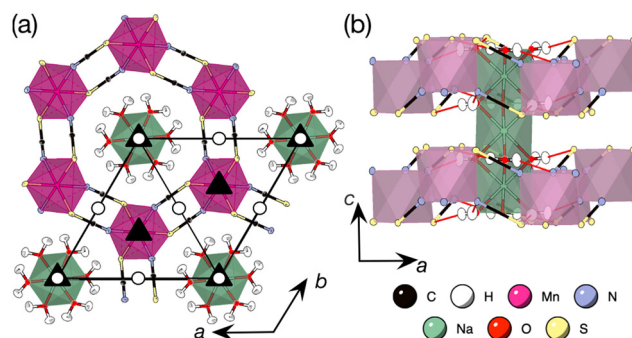
Fig. 1 Neutron single crystal structure of [Na(OH$_2$)$_3$]Mn(NCS)$_3$ (D19 at the ILL, 25 K).[17] (a) View along the c axis. Space group diagram for $P\bar{3}$ overlaid, $\bar{1}$: white circle, 3: black triangle. (b) View along the b axis. Hydrogen bonds shown as red lines.

ordering may break the centre of symmetry and hence induce simultaneous magnetic and electric order (type II multiferroicity).[22] Although the structure of this compound has been reported, because it is very sensitive to humidity, very little is known about its physical properties.[20] We report a method for the synthesis of large $[Na(OH_2)_3]Mn(NCS)_3$ single crystals (12 mm³) of suitable quality for neutron diffraction measurements, which mitigates the strong humidity dependence of this compound. Using a combination of bulk magnetic property measurements, low-temperature single crystal neutron diffraction and SHG measurements, we have determined its magnetic properties. We find that $[Na(OH_2)_3]Mn(NCS)_3$ orders with the classical honeycomb antiferromagnetic ground state, ordering into the centrosymmetric collinear antiferromagnetic $P\bar{3}'$ space group.

We synthesised $[Na(OH_2)_3]Mn(NCS)_3$ using a method adapted from that of Biedermann1998, using the salt metathesis of manganese(II) sulfate and barium thiocyanate with additional sodium thiocyanate in aqueous solution in a 1 : 1 : 1 ratio. After filtering the precipitated $BaSO_4$ and removing the water, a pale green-yellow powder was obtained, deliquescent in ambient conditions, which can be recovered from its own solution by heating at no more than 60 °C. The powder sample is also sensitive to dry environments, and will decompose to $Mn(NCS)_2$ and NaNCS on heating.

On concentration *in vacuo*, aqueous solutions of $[Na(OH_2)_3]$-$Mn(NCS)_3$ change colour sequentially from colourless to pale pink, pale green and eventually to aqua blue [Fig. S1, ESI†]. We found that the optimal concentration for crystal growth is when the solution is an intense green colour, just before it begins turning blue. More concentrated, blue, solutions very rapidly crystallised, which led to many smaller crystals. Less concentrated solutions were not sufficiently supersaturated for crystal growth [Fig. S2, ESI†]. On leaving this green solution to stand for 24 h at 7 °C we obtained large regular-hexagonal crystals. As the supersaturated solution absorbs water from the air, the concentration falls below the level required for optimal crystal growth after 24 h. The harvested crystals from this initial crystallisation were then used as seeds for future crystallisation with the growth solution being reconcentrated to the optimal concentrations. After nine iterations of seeded crystallisation we obtained pale green, hexagonal crystals of $[Na(OH_2)_3]$-$Mn(NCS)_3$ suitable for neutron diffraction experiments: 4 × 3 × 1 mm³ [Fig. 3(a)]. Due to the humidity sensitivity of this compound, we explored a variety of conditions for storage using saturated aqueous salt solutions to control the atmosphere: 54% $(Mg(NO_3)_{2(aq.)})$, 39% $(NaI_{(aq.)})$, 32% $(CaCl_{2(aq.)})$ and 23% $(KCH_3COO_{(aq.)})$.[23,24] We found that the crystals were indefinitely stable at 32% humidity (>23 months). We confirmed the phase purity of powder samples with powder X-ray diffraction and the quality of smaller single crystals was checked using ambient temperature X-ray single crystal diffraction.

Previous work has established that manganese thiocyanate compounds show moderately strong magnetic interactions,[18,19] and so to investigate the magnetic properties of $[Na(OH_2)_3]Mn$-$(NCS)_3$ and uncover any magnetic phase transitions, we carried
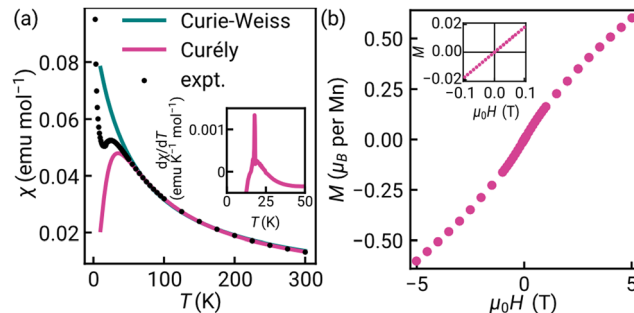

Fig. 2 (a) Magnetic susceptibility, χ measured from 2–300 K (black), with the high temperature fits using the Curie–Weiss (teal) and Curély equation (pink) for a classical honeycomb magnet. Inset: Temperature derivative of the susceptibility in the vicinity of the transition. (b) Isothermal magnetisation data, measured between +5.00 and −5.00 T at 2 K. Inset: Close-up of data between +0.1 and −0.1 T.

out magnetic susceptibility ($\mu_0 H = 0.01$ T) and isothermal magnetisation measurements on a powder sample (2 K, −5 to +5 T). We found that the magnetic susceptibility increases on cooling until a broad maximum is reached around 25 K. Below this temperature, the susceptibility decreases until a sharp drop at the ordering temperature, $T_N = 18.1(6)$ K [Fig. 2(a)]. The temperature dependence of the moment was fitted to the Curély model of a nearest neighbour classical honeycomb magnet,[12] using the following Hamiltonian:

$$\mathcal{H} = -\frac{1}{2}\sum_{i,j} JS_i \cdot S_j, \tag{1}$$

where $|S| = \sqrt{S(S+1)}$, and the sum is only over nearest neighbours. In this convention, antiferromagnetic superexchange will give negative J. We fitted the data over the full temperature range, with an additional $1/T$ term to account for paramagnetic impurities due to sample hydration, giving $J = -10.0(2)$ K and $g = 1.8$ with $7.0(2)\%$ paramagnetic impurities. We also fitted just the high temperature regime ($T > 60$ K), using both the Curély model, giving $J = -11.07(4)$ K, $g = 2.02$, and using the Curie–Weiss model which gives a Curie–Weiss temperature, $\theta_{CW} = -51.4(1.4)$ K, equivalent to $J = -17.4(5)$ K and $g = 2.09$, the overestimated Curie–Weiss temperature being typical of analysis of low-dimensional magnets. The presence of a small fraction of hydrated impurity means the extracted values of g are unreliable.

The isothermal magnetisation does not saturate up to $5.00(1)$ T, consistent with the moderately strong antiferromagnetism, and there is no observable hysteresis within the error limits of the measurements (<1 mT) [Fig. 2(b)]. A change in the gradient at 2.0(3) T is suggestive of a spin reorientation transition [Fig. S8, ESI†].

The combination of the negative θ_{CW} and lack of hysteresis in the isothermal magnetisation data, suggests that $[Na(OH_2)_3]$-$Mn(NCS)_3$ has ground-state antiferromagnetic order. If there is a ferromagnetic component due to spin canting, which could explain the up-turn in the low temperature susceptibility data, it must be small in magnitude.

This journal is © the Owner Societies 2024

Phys. Chem. Chem. Phys., 2024, **26**, 15844–15849 | **15845**

To determine the low temperature nuclear and magnetic structure of $[Na(OH_2)_3]Mn(NCS)_3$, single crystal neutron diffraction measurements were performed (D19, ILL).[17] Full datasets were collected above (25 K) and below (2 K) the ordering temperature of T_N = 18.1(6) K. The data at 25 K (λ = 1.45 Å, 631 independent reflections) could be integrated with the same space group as the reported structure at ambient temperature, $P\bar{3}$, indicating the absence of any structural transitions. The atom positions and anisotropic displacement parameters were refined freely, with a final χ^2 = 23.20, obtained by refinement using the FullProf programme.[25] From each H_2O molecule one hydrogen is directed towards a nitrogen, whilst the other hydrogen is positioned towards a sulfur atom with $\angle$ O–H$\cdots$N = 153.291(2)° and $\angle$ O–H$\cdots$S = 164.258(2)°. The distances of the hydrogens to the acceptor atoms are $d_{H1\cdots N}$ = 2.355(5) Å and $d_{H2\cdots S}$ = 2.326(7) Å, consistent with previous reports.[26]

In the low temperature dataset (2 K) all the Bragg reflections (651 unique reflections) could be indexed by the nuclear space group $P\bar{3}$, implying the propagation vector is k = (0,0,0). The potential magnetic space groups with this propagation vector were identified using the Bilbao Crystallographic Server,[27–29] $P\bar{3}'$, $P\bar{3}$, $P3$, $P\bar{1}'$, $P\bar{1}$ and $P1$ in BNS notation.[28] We initially focussed on the three maximal symmetry magnetic space groups: $P\bar{3}'$, $P\bar{3}$ and $P3$. Of these, the $P\bar{3}$ magnetic space group only allows for a collinear ferromagnetic order and so was neglected as it is inconsistent with our magnetic property measurements; $P\bar{3}'$ permits only collinear antiferromagnetic order and $P3$ allows antiferromagnetic, ferromagnetic or ferrimagnetic arrangement of the moments as it contains two distinct Mn(II) sites.

Refinements were carried out with both the $P\bar{3}'$ and $P3$ space groups. The results of the refinements provided comparable models with similar refinement statistics, χ^2 = 9.49 ($P\bar{3}'$) and χ^2 = 9.8 ($P3$) [Fig. S6 and S7, ESI†]. The significant difference between these models is the loss of the inversion centres in the $P3$ space group, which produces the two unique Mn sites. In both structures the Mn atoms are positioned on a 3-fold rotation axis and thus the moments are constrained to lie along c. The antiferromagnetic $P\bar{3}'$ model has a moment size, gS, of 4.9(2)μ_B per Mn, whereas in the $P3$ model, the magnitude of the two moments are $-3.4(3)$ and $5.4(2)\mu_B$. These moments were closely correlated, and were only stable during the refinements when the moments were constrained to refine between -5.0 and $5.0\mu_B$. This resulted in moments of $-4.0(2)$ and $3.9(2)\mu_B$. Within error these moments have the same magnitude, although any uncompensated moment would result in a net magnetisation along the c axis. We also investigated the potential for lower symmetry k = 0 orderings, with canted moments or significant magnetostructural distortions, which would require triclinic symmetry. We integrated the data with triclinic symmetry, which produced a cell which was trigonal within error, and then refined the magnetic and nuclear structures in $P\bar{1}'$ [Fig. S4 and Table S1, ESI†]. This model has a single Mn site, M = 4.1(2)μ_B, with the moment pointing primarily along the c axis with a significant canting, though the errors in this model prevent reliable determination of moment direction. The atomic coordinates and

displacement parameters were refined freely, however there was no evidence beyond error of any symmetry lowering beyond trigonal symmetry and the refinement fit was significantly worse than that for the higher symmetry models, with χ^2 = 51.3. We therefore concluded that the triclinic models were not required to describe this system.

To gain more detailed understanding of the transition we collected data between 2 and 25 K with 0.25 K steps to follow specific reflections. We focussed in particular on the 100 Bragg reflection, which has significant magnetic contribution in the magnetically ordered state. We fitted the intensity of this reflection to a power law:

$$I = M^2 = A(T_N - T)^{2\beta} + C, \qquad (2)$$

where A is a proportionality constant, T_N is the ordering temperature, β is a critical exponent and C the nuclear scattering intensity. We found for the 100 reflection that β = 0.31(3) and T_N = 18.94(7) K [Fig. 3(c)], which lies between the theoretical results for a two-dimensional Ising antiferromagnet (β = 0.125) and a three-dimensional Heisenberg antiferromagnet (β = 0.367).[30] This suggests that there is some degree of low dimensional character even in the vicinity of the transition, as found for other two dimensional magnets: $FeBr_3$ (β = 0.324),[31] $NiCl_2$ (β = 0.27)[32] and $FeCl_2$ (β = 0.29).[33] Other Bragg reflections, for example the 235 reflection, show almost no change in intensity with temperature as they have very limited contribution from magnetic scattering [Fig. S9, ESI†]. The nuclear structure at 2 K is
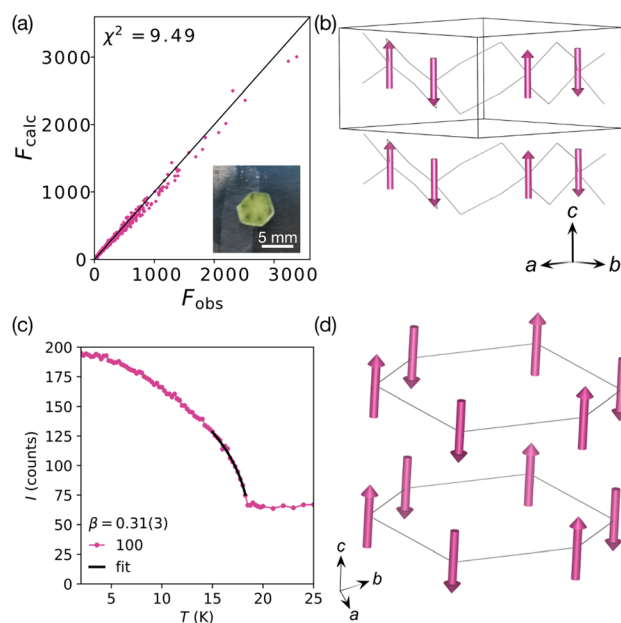

Fig. 3 Summary of the refined magnetic structure in $P\bar{3}'$ at 2 K (D19, ILL).[17] (a) F_{obs} against F_{calc} plot. Inset: The measured single crystal. (b) Magnetic structure viewed along the [110] direction showing the antiferromagnetic arrangement of moments (pink arrows). $[Mn(NCS)_3]^-$ framework is shown as a wireframe. (c) Temperature dependence of the 100 Bragg reflection, which has a significant magnetic contribution, fitted to a power law (black line), β = 0.31(3). (d) Alternate view of the magnetic structure, with the magnetic lattice (connecting Mn atoms) shown.

15846 | *Phys. Chem. Chem. Phys.*, 2024, **26**, 15844–15849

This journal is © the Owner Societies 2024

very similar to that at 25 K, with no statistically significant deviations in bond lengths.

Our refinements suggested that the magnetic structure is most likely the centrosymmetric antiferromagnetic $P\bar{3}'$, rather than the noncentrosymmetric weak ferromagnetic $P3$. To confirm this model and to determine if $[Na(OH_2)_3]Mn(NCS)_3$ is centrosymmetric in its ground state, we therefore carried out second harmonic generation measurements at 4 K and room temperature, along with variable temperature measurements between 4 and 30 K. Optical excitation was performed using Spectra Physics Spitfire Ace PA amplified laser system (40 fs pulses at a 1 kHz repetition rate) at 800 nm (<1 W average power) and 400 nm (<500 mW). We found no evidence of SHG signal generation, suggesting the compound is centrosymmetric. The results suggest that $[Na(OH_2)_3]Mn(NCS)_3$ retains its inversion centres, therefore ordering in the $P\bar{3}'$ magnetic space group, and providing further evidence that this compound is a good example of a classical Heisenberg honeycomb antiferromagnet.

The $[Mn(NCS)_3]^-$ layers of $[Na(OH_2)_3]Mn(NCS)_3$ stack uniformly along the c axis, in contrast to the ABC stacking found in $NaMnCl_3$.[34] We found no evidence of stacking faults, slip-stacking transitions or symmetry-lowering due to stacking, in contrast to van der Waals materials such as $MnPS_3$ and $RuCl_3$ which have monoclinic symmetry because of the layer sequence.[35,36] This is likely due to the infinite rod $[Na(OH_2)_3]_n^+$ countercation, which forces hydrogen bonds to the framework and force the layers to stack in alignment.

The importance of the trigonal symmetry of the cation, together with its templating hydrogen bonds, can be seen by comparison with $[1,3\text{-Im}]Mn(NCS)_3$ (1,3-Im = 1-ethyl-3-methyl imidazolium) which has the bulky 1,3-Im cation as the charge balance to the $[Mn(NCS)_3]^-$ honeycomb.[37] The 1,3-Im cation has no strong hydrogen bond donors and its size and bulk means the framework forms irregular hexagons. This distortion away from perfect symmetry is often found in molecular framework honeycomb magnets, for example $Co(N_3)_2(bpg)\cdot DMSO$ (bpg = 1,2-dipyridine-4-ethane-1,2-diol, DMSO = $SO(CH_3)_2$).[15,16] The $[Na(OH_2)_3]^+$ countercation rod is not unique to $[Na(OH_2)_3]Mn(NCS)_3$, occurring in a handful of other compounds, e.g. $[Na(OH_2)_3]_2$-$[TeBr_6]$.[38] Neutron diffraction allows a close look at the H-bond interactions between this cation and the framework.

The magnetic properties of $[Na(OH_2)_3]Mn(NCS)_3$ are quite distinct from the halide analogue $NaMnCl_3$, which orders at $T_N = 6.5$ K with ferromagnetic layers, coupled antiferromagnetically.[39] $[Na(OH_2)_3]Mn(NCS)_3$ has an ordering temperature almost three times as high as $NaMnCl_3$ ($T_N = 18.1(6)$ K) and the net magnetic interactions are also stronger, $\theta_{CW} = -51(1)$ K, compared to $NaMnCl_3$, $\theta_{CW} = -4.2$ K. The increase strength of interactions in the thiocyanate compared to the halide despite the significantly longer superexchange pathway (Mn–Cl–Mn compared to Mn–NCS–Mn) is consistent with investigations of the binary compounds.[18] This difference may be due to the harder NCS^- ligand having better orbital overlap with Mn^{2+} and the single-orbital nature of the superexchange pathway, rather than the two-orbital pathway in manganous chlorides.

Our results establish that $[Na(OH_2)_3]Mn(NCS)_3$ adopts the $P\bar{3}'$ space group, but it is worth exploring implications of the $P3$ magnetic symmetry with two uncompensated moments [Fig. S10, ESI†], particularly as analogous structures with different metals may adopt different ground states. $P3$ has no inversion centre and is polar, and so this structure (if it can be engineered in analogues or through application of stimulus e.g. strain) would have electrical polarisation produced directly by magnetic order (type II multiferroicity).[22] Generally, type II multiferroics adopt complex magnetic orderings, for example helical incommensurate states,[40] or with structural triangular lattice arrangements which introduce frustration, e.g. triangular $Sr_3NiTa_2O_9$[41] and $Ba_3MnNb_2O_9$.[42] It would be unusual for a collinear magnetic ordering to induce this behaviour, and even more so for a molecular framework. These results illustrate the importance of magnetic structure determination for understanding the function of magnetic molecular framework compounds, as also shown by other recent works on frameworks containing both Mn(II)[43–46] and other metals.[47–49]

In conclusion, we have determined the low temperature structure and magnetic properties of $[Na(OH_2)_3]Mn(NCS)_3$ by developing crystal growth methodology for this humidity sensitive compound. Neutron diffraction data permitted the hydrogen atoms to be located and hence the key role of the hydrogen bonding network in framework structuration. Refinement of single crystal neutron diffraction data shows that the compound magnetically orders in $P\bar{3}'$ magnetic space group, supported by SHG measurements for which we saw no signal at the wavelengths we excited, consistent with this centrosymmetric magnetic structure. The unusual low-symmetry trigonal space group exhibited in this compound suggests that investigations into the analogues incorporating metal ions which exhibit magnetic anisotropy (e.g. Co(II), Ni(II), Fe(II)) may lead to the complex spin structure and hence multiferroic behaviour. Substitutions for metals which form metal thiocyanate frameworks less sensitive to ambient humidity, e.g. Ni(II), may also lead to more straightforward methods to grow and store these compounds.

Author contributions

M. G. and E. B. synthesised the samples; M. G. grew the crystals; M. G. and M. J. C. carried out the magnetic measurements and the single crystal X-ray experiments; M. G., O. F., L. C. D. and M. J. C. carried out the neutron diffraction experiments and magnetic property analysis; T. B. G. and A. D. B. carried out the second harmonic generation measurements; M. G., L. C. D. and M. J. C. wrote the paper with contributions from all the authors.

Conflicts of interest

No conflicts of interest to declare.

Acknowledgements

References

1 B. Huang, G. Clark, E. Navarro-Moratalla, D. R. Klein, R. Cheng, K. L. Seyler, D. Zhong, E. Schmidgall, M. A. McGuire, D. H. Cobden, W. Yao, D. Xiao, P. Jarillo-Herrero and X. Xu, *Nature*, 2017, **546**, 270–273.

2 J. A. Sears, M. Songvilay, K. W. Plumb, J. P. Clancy, Y. Qiu, Y. Zhao, D. Parshall and Y.-J. Kim, *Phys. Rev. B: Condens. Matter Mater. Phys.*, 2015, **91**, 144420.

3 W. Yao, K. Iida, K. Kamazawa and Y. Li, *Phys. Rev. Lett.*, 2022, **129**, 147202.

4 S. Gao, M. A. McGuire, Y. Liu, D. L. Abernathy, C. D. Cruz, M. Frontzek, M. B. Stone and A. D. Christianson, *Phys. Rev. Lett.*, 2022, **128**, 227201.

5 S. Reschke, D. G. Farkas, A. Strinić, S. Ghara, K. Guratinder, O. Zaharko, L. Prodan, V. Tsurkan, D. Szaller, S. Bordács, J. Deisenhofer and I. Kézsmárki, *npj Quantum Mater.*, 2022, **7**, 1–7.

6 A. E. Thorarinsdottir and T. D. Harris, *Chem. Rev.*, 2020, **120**, 8716–8789.

7 Z. J. Zhong, N. Matsumoto, H. Okawa and S. Kida, *Chem. Lett.*, 1990, 87–90.

8 R. Pellaux, H. W. Schmalle, R. Huber, P. Fischer, T. Hauss, B. Ouaddiaf and S. Decurtins, *Inorg. Chem.*, 1997, **36**, 2301–2308.

9 C. Mathonière, S. G. Carling, D. Yusheng and P. Day, *J. Chem. Soc., Chem. Commun.*, 1994, 1551–1552.

10 I.-R. Jeon, B. Negru, R. P. Van Duyne and T. D. Harris, *J. Am. Chem. Soc.*, 2015, **137**, 15699–15702.

11 A. Rodríguez-Diéguez, J. Cano, R. Kivekäs, A. Debdoubi and E. Colacio, *Inorg. Chem.*, 2007, **46**, 2503–2510.

12 J. Curély, F. Lloret and M. Julve, *Phys. Rev. B: Condens. Matter Mater. Phys.*, 1998, **58**, 11465–11483.

13 A. Abhervé, M. Clemente-León, E. Coronado, C. J. Gómez-García and M. Verneret, *Inorg. Chem.*, 2014, **53**, 12014–12026.

14 M. Atzori, S. Benmansour, G. Mínguez Espallargas, M. Clemente-León, A. Abhervé, P. Gómez-Claramunt, E. Coronado, F. Artizzu, E. Sessini, P. Deplano, A. Serpe, M. L. Mercuri and C. J. Gómez García, *Inorg. Chem.*, 2013, **52**, 10031–10040.

15 X.-Y. Wang, L. Wang, Z.-M. Wang and S. Gao, *J. Am. Chem. Soc.*, 2006, **128**, 674–675.

16 M. A. S. Goher, J. Cano, Y. Journaux, M. A. M. Abu-Youssef, F. A. Mautner, A. Escuer and R. Vicente, *Chem. – Eur. J.*, 2000, **6**, 778–784.

17 M. Geers, L. Cañadillas-Delgado, M. J. Cliffe and Ó. Fabelo, ILL Experiment 5-41-1167, DOI: **10.5291/ILL-DATA.5-41-1167**.

18 E. N. Bassey, J. A. M. Paddison, E. N. Keyzer, J. Lee, P. Manuel, I. da Silva, S. E. Dutton, C. P. Grey and M. J. Cliffe, *Inorg. Chem.*, 2020, **59**, 11627–11639.

19 M. Geers, J. Y. Lee, S. Ling, O. Fabelo, L. Cañadillas-Delgado and M. J. Cliffe, *Chem. Sci.*, 2023, **14**, 3531–3540.

20 M. Biedermann, H. Hartung, H. Böhlandb and R. Matthäus, *Z. Naturforsch. B*, 1998, **53**, 416–422.

21 D. Zagorac, H. Müller, S. Ruehl, J. Zagorac and S. Rehme, *J. Appl. Crystallogr.*, 2019, **52**, 918–925.

22 D. Khomskii, *Physics*, 2009, **2**, 20.

23 L. Greenspan, *J. Res. Natl. Bur. Stand., Sect. A*, 1977, **81**, 89.

24 F. E. M. O'Brien, *J. Sci. Instrum.*, 1948, **25**, 73–76.

25 J. Rodríguez-Carvajal, *Phys. B*, 1993, **192**, 55–69.

26 J. P. M. Lommerse and J. C. Cole, *Acta Crystallogr.*, 1998, **B54**, 316–319.

27 M. I. Aroyo, J. M. Perez-Mato, D. Orobengoa, E. M. R. E. Tasci, G. de la Flor and A. Kirov, *Bulg. Chem. Commun.*, 2011, **43**, 183–197.

28 S. V. Gallego, E. S. Tasci, G. de la Flor, J. M. Perez-Mato and M. I. Aroyo, *J. Appl. Crystallogr.*, 2012, **45**, 1236–1247.

29 J. Perez-Mato, S. Gallego, E. Tasci, L. Elcoro, G. De La Flor and M. Aroyo, *Annu. Rev. Mater. Res.*, 2015, **45**, 217–248.

30 S. Blundell, *Magnetism in Condensed Matter*, Oxford University Press, Oxford, 2001.

31 A. Cole, A. Streeter, A. O. Fumega, X. Yao, Z.-C. Wang, E. Feng, H. Cao, J. L. Lado, S. E. Nagler and F. Tafti, *Phys. Rev. Mater.*, 2023, **7**, 064401.

32 P. A. Lindgard, R. J. Birgeneau, H. J. Guggenheim and J. Als-Nielsen, *J. Phys. C: Solid State Phys.*, 1975, **8**, 1059–1069.

33 W. B. Yelon and R. J. Birgeneau, *Phys. Rev. B: Solid State*, 1972, **5**, 2615–2621.

34 C. J. J. van Loon and G. C. Verschoor, *Acta Crystallogr., Sect. B: Struct. Crystallogr. Cryst. Chem.*, 1973, **29**, 1224–1228.

35 E. Ressouche, M. Loire, V. Simonet, R. Ballou, A. Stunault and A. Wildes, *Phys. Rev. B: Condens. Matter Mater. Phys.*, 2010, **82**, 100408.

36 R. D. Johnson, S. C. Williams, A. A. Haghighirad, J. Singleton, V. Zapf, P. Manuel, I. I. Mazin, Y. Li, H. O. Jeschke, R. Valentí and R. Coldea, *Phys. Rev. B: Condens. Matter Mater. Phys.*, 2015, **92**, 235119.

37 T. Peppel and M. Köckerling, *IUCrData*, 2019, **4**, x191659.

38 W. Abriel, *Z. Naturforsch. B*, 1983, **38**, 1543–1547.

39 N. Fedoseeva, I. Spevakova, G. Petrakovskii, V. Chuev and S. Petrov, *J. Magn. Magn. Mater.*, 1980, **15**, 539–541.

40 T. Kimura, J. C. Lashley and A. P. Ramirez, *Phys. Rev. B: Condens. Matter Mater. Phys.*, 2006, **73**, 220401.

41 M. Liu, H. Zhang, X. Huang, C. Ma, S. Dong and J.-M. Liu, *Inorg. Chem.*, 2016, **55**, 2709–2716.

42 M. Lee, E. S. Choi, X. Huang, J. Ma, C. R. Dela Cruz, M. Matsuda, W. Tian, Z. L. Dun, S. Dong and H. D. Zhou, *Phys. Rev. B: Condens. Matter Mater. Phys.*, 2014, **90**, 224402.

43 J. M. Bulled, J. A. M. Paddison, A. Wildes, E. Lhotel, S. J. Cassidy, B. Pato-Doldán, L. C. Gómez-Aguirre, P. J. Saines and A. L. Goodwin, *Phys. Rev. Lett.*, 2022, **128**, 177201.

44 S. Calder, R. Baral, N. Narayanan and L. D. Sanjeewa, *Phys. Rev. Mater.*, 2023, **7**, 124408.

15848 | *Phys. Chem. Chem. Phys.*, 2024, **26**, 15844–15849

This journal is © the Owner Societies 2024

45 H. C. Walker, H. D. Duncan, M. D. Le, D. A. Keen, D. J. Voneshen and A. E. Phillips, *Phys. Rev. B*, 2017, **96**, 2–7.

46 J. L. Manson, Q.-z Huang, J. W. Lynn, H.-J. Koo, M.-H. Whangbo, R. Bateman, T. Otsuka, N. Wada, D. N. Argyriou and J. S. Miller, *J. Am. Chem. Soc.*, 2001, **123**, 162–172.

47 J. Pitcairn, A. Iliceto, L. Cañadillas-Delgado, O. Fabelo, C. Liu, C. Balz, A. Weilhard, S. P. Argent, A. J. Morris and M. J. Cliffe, *J. Am. Chem. Soc.*, 2023, **145**, 1783–1792.

48 J. López-Cabrelles, S. Mañas-Valero, I. J. Vitórica-Yrezábal, P. J. Bereciartua, J. A. Rodríguez-Velamazán, J. C. Waerenborgh, B. J. C. Vieira, D. Davidovikj, P. G. Steeneken, H. S. J. van der Zant, G. Mínguez Espallargas and E. Coronado, *Nat. Chem.*, 2018, **10**, 1001–1007.

49 L. Cañadillas-Delgado, L. Mazzuca, O. Fabelo, J. Rodríguez-Carvajal and V. Petricek, *Inorg. Chem.*, 2020, **59**, 17896–17905.

This journal is © the Owner Societies 2024

Phys. Chem. Chem. Phys., 2024, **26**, 15844–15849 | **15849**